Nature of electrically detected magnetic resonance in highly nitrogen-doped 6*H*-SiC single crystals

M. Holiatkina,[1] A. Solodovnyk,[2,3] O. Laguta,[3] P. Neugebauer,[3] E. Kalabukhova,[4] and D. Savchenko[1,5,*]

[1]*Department of General Physics and Modeling of Physical Processes, National Technical University of Ukraine "Igor Sikorsky Kyiv Polytechnic Institute," Prospekt Beresteiskyi 37, Kyiv, 03056, Ukraine*

[2]*Department of Engineering Science and Mechanics, The Pennsylvania State University, University Park, Pennsylvania 16802, USA*

[3]*Central European Institute of Technology, Brno University of Technology, Purkynova 656/123, Brno, 61200, Czech Republic*

[4]*Department of Optics and Spectroscopy, V. E. Lashkaryov Institute of Semiconductor Physics NAS of Ukraine, Prospekt Nauky 41, Kyiv, 03028, Ukraine*

[5]*Technical Center NAS of Ukraine, 13 Pokrovs'ka Street, 04070 Kyiv, Ukraine*

(Received 6 June 2024; revised 22 August 2024; accepted 22 August 2024; published 9 September 2024)

This work focuses on unraveling electron paramagnetic resonance (EPR) and electrically detected magnetic resonance (EDMR) properties of *n*-type 6*H* silicon carbide (SiC) single crystals with high concentrations of uncompensated nitrogen (N) donors, which is essential for fundamental understanding of spin-related phenomena, developing spin-based devices, optimizing materials and devices, and advancing research in quantum information and spintronics. Utilizing low-temperature multifrequency EPR spectroscopy (9.4–395.12 GHz), we identified two intense signals labeled as S line and S1 line in the 6*H*-SiC crystals with N_D–$N_A \approx 8 \times 10^{18}$ and 4×10^{19} cm^{-3}. In addition, in 6*H*-SiC crystals with N_D–$N_A \approx 8 \times 10^{18}$ cm^{-3}, a low-intensity triplet from N donors substituting the quasicubic "k2" nonequivalent position (N_{k2}) was observed. The S line [$g_\perp = 2.0029(2)$, $g_\parallel = 2.0038(2)$] was assigned to the exchange interaction of conduction electrons and N_{k2}, while the S1 line [$g_\perp = 2.0030(2)$, $g_\parallel = 2.0040(2)$] is caused by the exchange spin coupling of localized N donors at the "k1" and "k2" positions. The S1 line was observed in high-frequency EDMR spectra of 6*H*-SiC with N_D–$N_A \approx 8 \times 10^{18}$ cm^{-3}, and its emergence was explained by an enhancement of the hopping conductivity due to the EPR-induced temperature increase mechanism. No EDMR spectra were found to occur in the 6*H*-SiC crystals with N_D–$N_A \approx 4 \times 10^{19}$ cm^{-3}, which is close to the critical donor concentration value for a semiconductor-metal transition. Thus it can be concluded that this N donor concentration is too high for the appearance of spin-dependent scattering and too low for the emergence of EPR-induced hopping mechanisms in 6*H*-SiC.

DOI: 10.1103/PhysRevB.110.125205

I. INTRODUCTION

Silicon carbide (SiC), a wide band gap IV-IV semiconductor compound containing silicon (Si) and carbon (C), is a cornerstone in the industrial scale production of large-size single crystalline wafers and epilayers of high quality, leading to the wide spread of high-performance SiC-based modules and devices. SiC materials offer a number of unique properties, such as high thermal conductivity, high breakdown voltage, and low on-resistance, which allow SiC-based devices operating at high temperatures and voltages to possess high light output, high efficiency, high thermal stability, high power handling capability, and high operating temperatures.

This makes SiC suitable for sensors, actuators, and other microdevices requiring resilience in extreme conditions [1] and contributes to developing smaller, lighter solar inverters [2]. SiC-based power devices are widely used in high-power applications such as electric vehicles [3], renewable energy systems, and industrial motor drives. SiC LEDs are used in automotive, street, and indoor lighting applications [4]. Moreover, SiC-based devices are used in radar [5] and satellite communication systems [6]. Most recent publications concerning future potential applications of SiC material relate to using SiC as a multiqubit memory and quantum computing platform [7]; for quantum information processing [8]; and for quantum sensing of magnetic, electric fields, and temperature at the nano- and microscale [9,10].

SiC exhibits polymorphism with various polytypes, representing different structures of the same chemical compound. There are over 250 polytypes of SiC, each characterized by a unique stacking sequence of Si-C bilayers. The most known SiC polytypes are cubic (3*C*), hexagonal (2*H*, 4*H*, 6*H*), and rhombohedral (15*R*).

Among other SiC polytypes, the 6*H* stands out owing to its stability, wide band gap, high thermal conductivity, mechanical strength, and optical properties. According to [11],

*Contact author: dariyasavchenko@gmail.com

due to the freeze-out of deep donor levels, the ionized impurity scattering in 6*H*-SiC is reduced, and the role of phonon scattering is enhanced, relative to the 3*C* and 4*H* polytypes. Moreover, 6*H*-SiC should provide a reduced electron trapping (compared to 4*H*-SiC) due to the larger conduction band offset at the SiC/SiO_2 interface in metal-oxide-semiconductor electron devices [12]. These benefits contribute to the industrial application of 6*H*-SiC, including power electronics, automotive, aerospace, and optoelectronics. In past years, 6*H*-SiC has been widely used as substrates for the growth of GaN crystals [13], graphene [14], AlGaN/GaN high-electron-mobility transistors [15], AlGaN thin film cathodes [16], thin MgO films [17], and diamond films [18]. Recently, a device comprising a 6*H*-SiC-based double gate Schottky barrier FET with two cavities for detecting biomolecules was proposed [19]. In [20], the advantage of using 6*H*-SiC over other solid-state materials in quantum/solid-state magnetometers was shown.

Nitrogen (N) is the principal uncontrolled *n*-type dopant impurity in all SiC polytypes. According to [21], one of the main issues of the usage of N-vacancy (NV) centers in SiC in quantum calculations and sensorics systems is the control of paramagnetic N donor content and spin couplings, leading to the loss of coherent properties of NV centers. Since N donors in SiC have shallow levels in the band gap, their wave functions are highly delocalized and unpaired donor electrons can be delocalized on C and Si atoms. Moreover, the polytype and donor impurity site in the SiC lattice affect the ratio of the delocalization degree.

Heavily N-doped 6*H*-SiC wafers are essential for fabricating high-power [Schottky diodes, metal-oxide-semiconductor field-effect transistors (MOSFETs)] and high-frequency [High Electron Mobility Transistors (HEMTs) and Bipolar Junction Transistors (BJTs)] devices, and rf power amplifiers. Moreover, recently it was reported that the resistivity nonuniformity in the grown SiC crystals considerably decreases when the SiC crystal is highly N doped allowing the obtaining of homogeneously nitrogen-doped SiC crystals with uniform electrical resistivities [22]. Thus, studying the relationship between the magnetic and electrical properties of N donors in such low-resistivity material is highly important both for electronic and quantum device fabrication.

Electron paramagnetic resonance (EPR) spectroscopy is widely applied to study the electronic and magnetic properties in SiC materials. In electrically detected magnetic resonance (EDMR) measurements, one detects EPR through a change in sample current, so this technique is sensitive to defects taking part in electronic transport. As a result, studying the origin of EDMR signals and their correlation with conventional EPR signals in SiC.

While the EDMR data on SiC material have been extensively studied in 4*H*-SiC MOSFETs [23–25], transistors [26–28], Si vacancies and interface defects [29,30], C dangling bonds [31,32], radiation-induced defects that occurred in 4*H*-SiC/SiO_2, 6*H*-SiC LEDs [33], and nanostructures [34], there remains a significant gap in our knowledge—the lack of EDMR data on spin defects in bulk SiC crystals [9].

We recently reported an observation of an EDMR signal in 15*R*-SiC single crystals with an uncompensated N donor concentration of about $5 \times 10^{18}\,\mathrm{cm}^{-3}$ at low temperatures [35]. The emergence of the EDMR signal was attributed to exchange-coupled N donors and explained by the spin-flip hops process and mechanism of EPR-induced temperature increase.

The *X*-band (~ 9 GHz) EDMR investigation of crystalline 4*H*-SiC with N_D–$N_A \approx 10^{18}\,\mathrm{cm}^{-3}$ and 6*H*-SiC with N_D–$N_A \approx 2 \times 10^{18}\,\mathrm{cm}^{-3}$ in Ref. [36] allowed the author to conclude that the mechanism of EPR-induced temperature increase leads to the appearance of a low-temperature EDMR signal.

At the same time previous temperature-dependent *X*-band EPR studies of highly N-doped 6*H*-SiC crystals with uncompensated N donor concentration exceeding $10^{19}\,\mathrm{cm}^{-3}$ revealed at least two overlapping signals at low temperatures: one signal was related to the exchange coupling among localized and nonlocalized electrons, and another one was tentatively attributed to the exchange coupling between localized N donors substituting hexagonal (h) and cubic (k) positions [37].

Since no spin Hamiltonian parameters were presented for the observed EDMR signal in Ref. [36], the relationship with observed EPR and EDMR spectra was not established and, as a result, the nature of the EDMR signal responsible for electrical properties of highly N-doped 6*H*-SiC single crystals remains unknown.

In this work, by utilizing multifrequency EPR and EDMR spectroscopy, we aim to elucidate the nature of the spin-related phenomena and the impact of nitrogen doping on the electrical and magnetic properties of 6*H*-SiC single crystals.

II. MATERIALS AND METHODS

The *n*-type 6*H*-SiC single crystals with uncompensated N donor concentration N_D–$N_A \approx 8 \times 10^{18}\,\mathrm{cm}^{-3}$ ($4.5\,\mathrm{mm} \times 2\,\mathrm{mm} \times 0.5\,\mathrm{mm}$) and $4 \times 10^{19}\,\mathrm{cm}^{-3}$ ($6\,\mathrm{mm} \times 2.1\,\mathrm{mm} \times 0.5\,\mathrm{mm}$) (determined by Hall effect at room temperature) were grown by a modified Lely method [38] utilizing polycrystalline SiC as source material with 1.2 mm/h growth rate on the [0001] Si face at 2200 °C−2400 °C and Ar pressure of 30–50 mbar.

Figure 1 represents the 6*H*-SiC crystal structure, having two nonequivalent quasicubic positions ("k1" and "k2") and one hexagonal ("h"). N donors substitute these nonequivalent positions with deep energy levels in the 6*H*-SiC band gap: 81 meV for N substituting the h position (N_h), 137.6 meV for N substituting the k1 position (N_{k1}), and 142.4 meV for N substituting the k2 position (N_{k2}) [39].

X-band ($\nu \sim 9.4$ GHz) continuous wave EPR spectra in 6*H*-SiC single crystals were measured using a Bruker ELEXSYS E580 spectrometer equipped with a Bruker ER 4122 SHQE SuperX High-Q cylindrical TE_{011} cavity and variable temperature helium-flow cryostat ER 4112HV. The following parameters were used: microwave (MW) power level of 0.4743 mW, modulation frequency of 100 kHz, modulation amplitude of 0.1 mT, conversion time of 70 ms, and spectral resolution of 2048 points. The samples were fixed on a fused quartz rod with a diameter of 4 mm. As a reference sample, the 1,1-*diphenyl*-2-*picrylhydrazyl* free radical ($g = 2.0036$) was used.

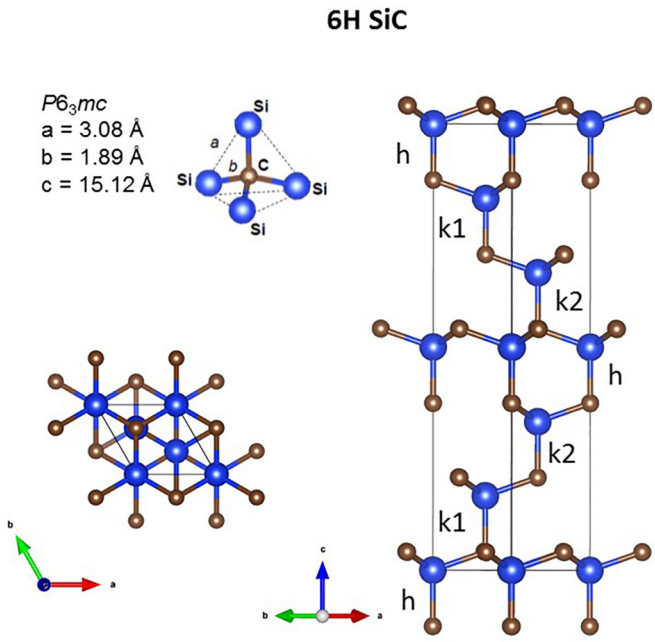

FIG. 1. The 6*H*-SiC crystal structure drawn using the data from Ref. [40] in the VESTA 3.5.2 program [41]. The **c** axis is along the [0001] direction.

High-frequency EPR (from 100 to 395.12 GHz) and EDMR (100 GHz) spectra were measured on a THz FraScan Spectrometer (CEITEC BUT, Brno, Czech Republic) using a chip sample holder [42,43] and two different MW sources [and a set of passive frequency multipliers (3×) for 395.12 GHz] utilizing a superconductive cryogen-free magnet, Cryogenic Ltd, UK. High-frequency EPR spectra were measured with the following parameters: magnetic field sweep rate: 0.1–0.18 mT/s; time constant: 30 ms; modulation frequency: 2.8–4.3 kHz; modulation amplitude: 0.24–0.4 mT; MW power level of ∼1−2 mW. High-frequency EDMR spectra were recorded utilizing the detection scheme from [44] with the following parameters: magnetic field sweep rate: 0.1 mT/s; time constant: 30 ms; magnetic field modulation amplitude: 0.24–0.5 mT; magnetic field modulation frequency: 734 Hz; bias voltage: +4.88 V; MW power level of ∼125 mW. For EDMR measurements, the sample was contacted with Ag-based paint onto a glass substrate with Au contact pads. As a reference sample for high-frequency EPR, we utilized Cr^{3+} in MgO with $g = 1.9797$.

For the EPR spectra simulation, we have used the "pepper" function from the EASYSPIN 5.2.36 toolbox [45] utilizing the spin Hamiltonian (expressed in angular frequency units),

$$\hat{H} = \mu_B \mathbf{BgS}/\hbar - g_n \mu_n \mathbf{BI}/\hbar + \sum_i \mathbf{SA}_i\mathbf{I}_i + \mathbf{IPI}, \quad (1)$$

where μ_B is the Bohr magneton; $\mathbf{B} = (0, 0, B_z)$ is the externally applied magnetic field; B_0 is the resonance magnetic field position, **g** is the electron *g*-tensor; **S** is the electron spin operator; $\hbar = h/2\pi$ is the reduced Planck constant; g_n is the nuclear *g* factor; μ_n is the nuclear magneton; $\mathbf{I}_i$ is the nuclear spin operator of the *i*th nucleus; $\mathbf{A}_i$ is the hyperfine interaction tensor of the *i*th nucleus; **P** is the nuclear quadrupole interaction tensor. In the case of axial **g**-tensor symmetry $g_1 = g_\parallel$, $g_2 = g_3 = g_\perp$ and $A_\parallel = a_l + 2b_l$, $A_\perp = a_l - b_l$ (a_l is the isotropic hyperfine interaction constant of the *l*th atom; b_l is the anisotropic hyperfine interaction constant of the *l*th atom).

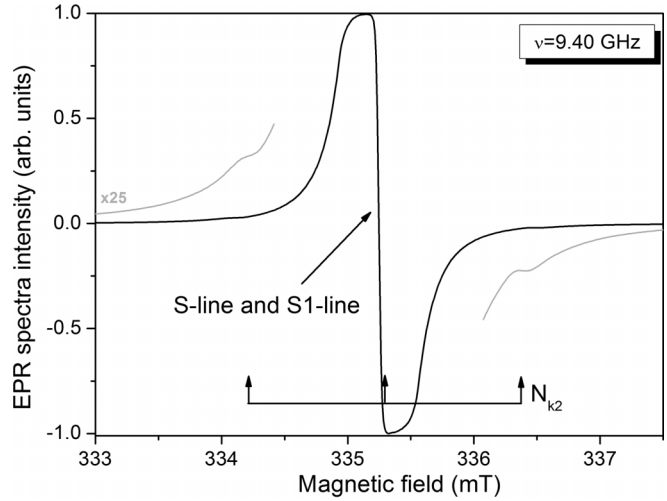

FIG. 2. The *X*-band EPR spectrum measured in 6*H*-SiC single crystals with N_D–$N_A \approx 8 \times 10^{18}\,\mathrm{cm}^{-3}$ at $T = 5\,\mathrm{K}$ and $\mathbf{B} \parallel \mathbf{c}$.

For the paramagnetic center having $S = 1/2$ and $I = 0$, one should consider the first and second terms of Eq. (1) only, and a single line in the EPR spectrum is observed. For the paramagnetic center having $S = 1/2$ and $I = 1$, all the terms of Eq. (1) should be considered, and a triplet ($2I + 1 = 3$ lines) in the EPR spectrum is detected.

III. RESULTS AND DISCUSSION

A. EPR measurements

Figure 2 represents the typical *X*-band ($\nu \sim 9.4$ GHz) EPR spectrum recorded in 6*H*-SiC single crystals with N_D–$N_A \approx 8 \times 10^{18}\,\mathrm{cm}^{-3}$ at $T = 5\,\mathrm{K}$. The central part of the EPR spectrum reveals two overlapping signals labeled as S line and S1 line with $S = 1/2$, $I = 0$ previously reported in 6*H*-SiC single crystals with N_D–N_A ranging from 1×10^{19} to $4 \times 10^{19}\,\mathrm{cm}^{-3}$ [37]. The S-line temperature behavior corresponds to those obtained for the conduction electron spin resonance (CESR) signal [37]. In addition, a triplet of small intensity (with much lower spin density than the central signals) arising from N_{k2} donors ($S = 1/2$, $I = 1$) [46] is seen. The N_h and N_{k1} donors (with shallower energy levels in the band gap than N_{k2}) are ionized in these samples; therefore, no EPR spectra were observed from these centers.

In 6*H*-SiC single crystal samples with N_D–$N_A \approx 4 \times 10^{19}\,\mathrm{cm}^{-3}$, only S-line and S1-line signals were observed in EPR spectra at $T = 5\,\mathrm{K}$, and no signals from N_{k2} donors. According to Ref. [44], a multifrequency EPR approach was utilized to resolve the overlapping signals. Figure 3 demonstrates the experimental and simulated EPR spectra in 6*H*-SiC single crystals having N_D–$N_A \approx 8 \times 10^{18}\,\mathrm{cm}^{-3}$ at different MW frequencies in two magnetic field orientations. Applying high MW frequencies, we could distinguish the spin Hamiltonian parameters for the S line and S1 line at such high

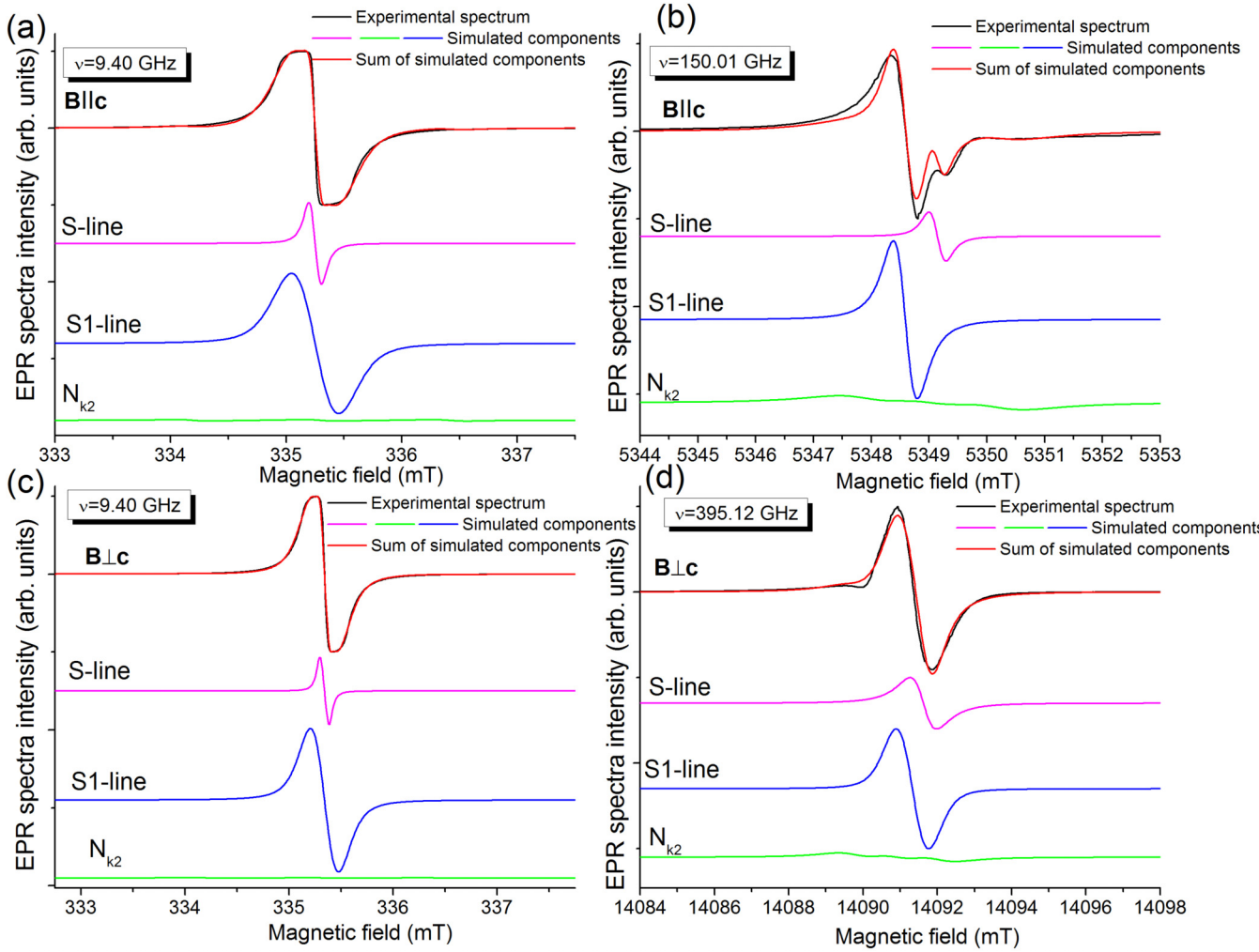

FIG. 3. EPR spectra recorded in 6*H*-SiC single crystals with N_D–$N_A \approx 8 \times 10^{18}$ cm^{-3} at $\nu = 9.40$ GHz **B** ∥ **c** (a), $\nu = 150.01$ GHz, **B** ∥ **c** (b), $\nu = 9.40$ GHz, **B**⊥**c** (c), $\nu = 395.12$ GHz, and **B**⊥**c**. $T = 5$ K. Black solid lines represent experimental spectra. Magenta, blue, and green solid lines are simulated spectral components using Eq. (1), and red solid lines show the sum of simulated spectral components.

N concentration; the free electrons, which are ionized from N donors at "h" and "k1" sites in 6*H*-SiC, may screen the localized N_{k2} electrons and, thus, lead to the ionization of the deeper N_{k2} donors [47].

Table I summarizes the spin Hamiltonian parameters of the observed paramagnetic centers. It shows that the hyperfine coupling constants for the N_{k2} center are slightly lower than those found previously in 6*H*-SiC single crystals with N_D–$N_A \approx 10^{17}$ cm^{-3} [46]. This effect can be elucidated by the possible deviation from Si/C stoichiometry in highly N-doped 6*H*-SiC single crystals.

Considering the obtained g values for the S line, this paramagnetic center should be assigned to the exchange coupling of conduction electrons and N_{k2}. The difference in the spin Hamiltonian parameters for the S line at $T = 5$ K in this work from those obtained for the CESR signal at the X band

TABLE I. The spin Hamiltonian parameters for paramagnetic centers in highly N-doped 6*H*-SiC single crystals at $T = 5$ K, along with the literature data.

Paramagnetic center	N_D–N_A (cm^{-3})	Temperature range	$g_\perp$	$g_\parallel$	$A_\perp$ (mT)	$A_\parallel$ (mT)	Reference
N_{k2}	8×10^{18}	$T < 25$ K	2.0030(2)	2.0037(2)	1.11	1.11	This work
N_{k2}	10^{17}	$T < 80$ K	2.0030(3)	2.0037(3)	1.19	1.19	[46]
N_{k1}	10^{17}	$T < 80$ K	2.0026(3)	2.0040(3)	1.2	1.2	[46]
S line	8×10^{18}	$T < 150$ K	2.0029(2)	2.0038(2)	—	—	This work
CESR signal	$10^{19} - 4 \times 10^{19}$	$T < 150$ K	2.0034(3)	2.0047(3)	—	—	[37]
S1 line	8×10^{18}	$T < 25$ K	2.0030(2)	2.0040(2)	—	—	This work
S1 line	$5 \times 10^{18} - 4 \times 10^{19}$	$T < 25$ K	2.0031(3)	2.0045(3)	—	—	[37,48]

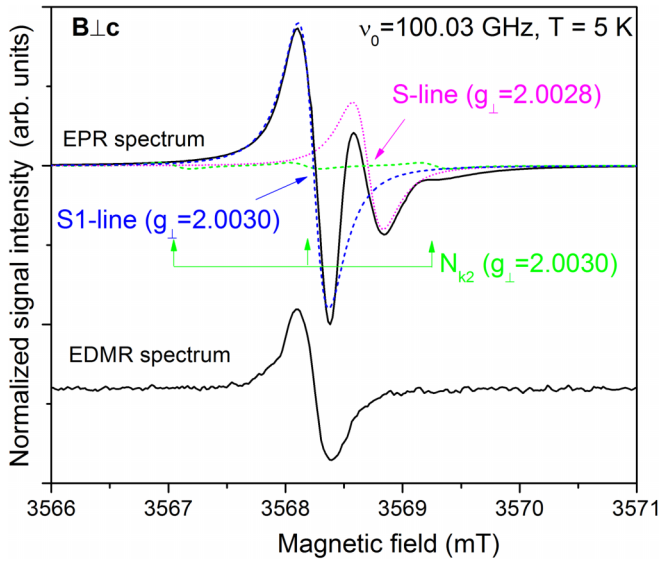

FIG. 4. EPR and EDMR spectra recorded in 6*H*-SiC single crystals with N_D–$N_A \approx 8 \times 10^{18}\,cm^{-3}$ at $\nu = 100.03$ GHz, $\mathbf{B}\perp\mathbf{c}$, and $T = 5$ K. Black solid lines represent experimental spectra. Magenta, blue, and green solid lines are simulated spectral components using Eq. (1). The spectral intensity was normalized to its maximum value.

[37] should be attributed to the fact that the multifrequency EPR approach allows us to establish the spin Hamiltonian parameters more precisely.

The S1 line is observed at $T < 25$ K [37] and has $g_\perp = 2.0030(2)$, which coincides with the $g_\perp$ value for N_{k2}, and $g_\parallel = 2.0040(2)$ corresponding to the $g_\parallel$ value for N_{k1}. Therefore, we can conclude that the S1 line should be related to the exchange spin coupling of localized N_{k1} and N_{k2} donors in highly N-doped 6*H*-SiC.

The conclusions made above are also confirmed by the fact that the temperature interval for the appearance of the S line ($T < 150$ K) corresponds to the temperature range where electron transitions from impurity levels to the conduction band occur in 6*H*-SiC single crystals with N_D–$N_A \approx 1 \times 10^{19} - 4 \times 10^{19}\,cm^{-1}$ [49] [at $T > 150$ K the cavity Q factor is too low to adjust the automatic frequency control (AFC) and record the EPR spectrum from the S line]. At the same time, the temperature range for S1-line emergence ($T < 25$ K) matches the range for the electron hopping process over N impurity atoms in the D^0 bands taking place in 6*H*-SiC with N_D–$N_A \approx 1 \times 10^{19} - 4 \times 10^{19}\,cm^{-1}$ [49].

B. EDMR measurements

We have observed a single line in high-frequency EDMR spectra of 6*H*-SiC single crystals with N_D–$N_A \approx 8 \times 10^{18}\,cm^{-3}$ at $T < 10$ K. The temperature behavior, power dependence, and current dependence of this EDMR signal (see Supplemental Material [50]) correspond to those previously reported for 15*R*-SiC with N_D–$N_A \approx 5 \times 10^{18}\,cm^{-3}$ in Ref. [35], 4*H*-SiC with N_D–$N_A \approx 10^{18}\,cm^{-3}$, and 6*H*-SiC with N_D–$N_A \approx 2 \times 10^{18}\,cm^{-3}$ in Ref. [36].

Figure 4 shows the comparison of high-frequency EPR and EDMR spectra recorded at $T = 5$ K in 6*H*-SiC single crystals with N_D–$N_A \approx 8 \times 10^{18}\,cm^{-3}$ at $\nu = 100.03$ GHz, $\mathbf{B}\perp\mathbf{c}$. It can be seen that the resonance field position of a single EDMR line corresponds to the S1 line detected in the EPR spectrum. This fact agrees with our previously published results in 15*R*-SiC single crystals having N_D–$N_A \approx 5 \times 10^{18}\,cm^{-3}$, where the EDMR line was also related to exchange interaction between identical N_{k1} donors [35].

Moreover, according to Ref. [36], hopping conductivity is the dominant charge transport process at low temperatures in SiC crystals with N_D–N_A from 10^{18} to $10^{19}\,cm^{-3}$. In 6*H*-SiC having N_D–$N_A \approx 2 \times 10^{18}\,cm^{-3}$, the Fermi level lies near the N energy level at quasicubic lattice sites, and thus hopping should take place only between quasicubic site donors.

In contrast to Ref. [36], where both intense EDMR line and N donors were observed in the EDMR spectrum in 6*H*-SiC having N_D–$N_A \approx 2 \times 10^{18}\,cm^{-3}$, we observe only one EDMR line in our samples, which can be elucidated by the higher N donor content in our samples.

Thus we may conclude that we observe the same EDMR signal as was previously detected in 6*H*-SiC having N_D–$N_A \approx 2 \times 10^{18}\,cm^{-3}$ [36] where its appearance was considered based on the following microscopic process: at resonance, the spin system absorbs energy, through spin lattice this energy is transferred to the lattice surroundings, leading to a temperature increase at resonance conditions, enabling additional hopping. So, the EDMR mechanism in our samples can be related to an enhancement of the hopping conductivity due to the EPR-induced temperature increase process as responsible for the EDMR signal.

In [36], it was proposed that the EDMR mechanism varies with the N donor concentration in SiC. For EDMR signals caused by the spin-dependent donor-acceptor recombination mechanism, the N_D–N_A should lie from 10^{11} to $10^{13}\,cm^{-3}$. The EDMR signal, caused by hopping conductivity due to the EPR-induced temperature increase, occurs when N_D–N_A lies from 10^{18} to $10^{19}\,cm^{-3}$. The samples with N_D–N_A of about $10^{15}\,cm^{-3}$ should not reveal EDMR signals since this concentration is too large for the spin-dependent recombination mechanism (the recombination rate is too high as compared to the EPR rate) and is too low for hopping conductivity (the average distance between N donors is too large) [36]. For the N_D–N_A concentrations higher than the critical donor concentration value for the semiconductor-metal transition, the appearance of the EDMR signal should be related to the mechanism of spin-dependent scattering at the neutral impurities [51]. Thus the semiconductor-metal transition separates the region between EPR-induced and spin-dependent hopping.

According to the Mott criterion, the semiconductor-metal transition occurs when $N_c^{1/3} a_B \approx 0.3$ (N_c is the critical donor concentration; a_B is the Bohr radius). We did not detect EDMR signals in 6*H*-SiC single crystals having N_D–$N_A \approx 4 \times 10^{19}\,cm^{-3}$ which is close to $N_c \approx 7 \times 10^{19}\,cm^{-3}$ for 6*H*-SiC ($a_B \approx 7.2$ Å). Therefore, we can conclude that when N_D–N_A is close to N_c, it is still too low for the spin-dependent scattering mechanism to occur, whereas it is too high for the appearance of the EPR-induced hopping process, and no EDMR signal in 6*H*-SiC can be detected.

The fact that we do not see the EDMR signals in 6*H*-SiC single crystals with N_D–$N_A \approx 4 \times 10^{19}\,cm^{-3}$ is also related to the lower conductivity of these samples which prevents the

detection of the EDMR signal. In Ref. [36], the author reported that in the 6*H*-SiC crystals with N_D–$N_A \approx 2 \times 10^{19}\,cm^{-3}$ and N_D–$N_A \approx 4 \times 10^{19}\,cm^{-3}$, the resistivity increased under MW irradiation, and this was explained by the fact that when N concentration is higher than N_c the donor states are delocalized and charge transport is bandlike. When the MW irradiation is applied, the mobility of the conduction electrons decreases leading to a resistivity enhancement. Furthermore, we have observed the same effect in 4*H*-SiC crystals with N_D–$N_A > N_c$.

It should be noted that the S line is characterized by a purely Lorentzian line shape, while the S1 line is described by the Voigtian line shape both in EPR and EDMR spectra. This is in agreement with an EDMR signal line shape observed for 6*H*-SiC single crystals with N_D–$N_A \approx 2 \times 10^{18}\,cm^{-3}$ [36], which was partly a Gaussian line shape due to inhomogeneous broadening and partly a Lorentzian one due to homogeneous contributions from the exchange interaction.

IV. CONCLUSIONS

The *n*-type 6*H*-SiC single crystals, grown by the modified Lely method, with uncompensated N donor concentration of 8×10^{18} and $4 \times 10^{19}\,cm^{-3}$, were examined by multifrequency EPR and EDMR techniques at $T = 5$ K.

Three paramagnetic centers were observed in the EPR spectra of 6*H*-SiC crystals with N_D–$N_A \approx 8 \times 10^{18}\,cm^{-3}$. The triplet of small intensity arises from N donors residing "k2" (N_{k2}) donors with $S = 1/2$, $I = 1$ and spin Hamiltonian parameters: $g_\perp = 2.0030(2)$, $g_\parallel = 2.0037(2)$, and $A_\perp = A_\parallel = 1.11$ mT. The slight decrease in hyperfine coupling constants for the N_{k2} center from those found previously in 6*H*-SiC single crystals having N_D–$N_A \approx 10^{17}\,cm^{-3}$ as $A_\perp = A_\parallel = 1.19$ mT was explained by the possible deviation from Si/C stoichiometry in highly N-doped 6*H*-SiC single crystals.

The intense signal of a Lorentzian line shape labeled as S line having $S = 1/2$, $I = 0$ and $g_\perp = 2.0029(2)$, $g_\parallel = 2.0038(2)$ was observed in EPR spectra at $T < 150$ K. Taking into account the previously published data this S line was attributed to the exchange interaction of conduction electrons and N_{k2}. Another intense signal of a Voigtian line shape labeled as S1 line characterized by $S = 1/2$, $I = 0$ and $g_\perp = 2.0030(2)$, $g_\parallel = 2.0040(2)$ was detected at $T < 25$ K in EPR spectra. Based on its spin Hamiltonian parameters, we assign this paramagnetic center to the exchange spin interaction of localized N_{k1} and N_{k2} donors.

In 6*H*-SiC single crystals having N_D–$N_A \approx 4 \times 10^{19}\,cm^{-3}$ the EPR spectrum consists of the S line and the S1 line, and no triplet line from the N_{k2} donor state was observed due to the free electron screening effect that occurs owing to ionization electrons from shallow N_h and N_{k1} donor levels.

The EDMR spectrum measured in 6*H*-SiC crystals having N_D–$N_A \approx 8 \times 10^{18}\,cm^{-3}$ revealed a single line attributed to the S1 line. The emergence of this EDMR signal is related to the enhancement of the hopping conductivity due to the effect of an EPR-induced temperature increase. This mechanism can be characterized as follows: at resonance conditions, the spin system absorbs MW energy, and then due to relaxation processes, this MW energy is transferred to the surroundings. Thus, at resonance conditions, the crystal is heated.

The 6*H*-SiC single crystals having N_D–$N_A \approx 4 \times 10^{19}\,cm^{-3}$ revealed no EDMR signal from the S line, which was explained by the fact that this concentration close to the critical donor concentration value for semiconductor-metal transition is too low for the spin-dependent scattering mechanism and it is too high for the EPR-induced hopping process.

The insights gained from the study regarding N donor interactions in 6*H*-SiC single crystals and their effects on electrical properties can be applied to designing high-power SiC-based electronics. This includes improving the performance and reliability of devices like MOSFETs, Schottky diodes, and high-frequency transistors, which are essential in electric vehicles, renewable energy systems, and industrial power management. Moreover, the obtained results are essential from the perspective of SiC usage in quantum applications.

ACKNOWLEDGMENTS

The authors are grateful to Prof. P. Lenahan (The Pennsylvania State University, USA) for useful comments and suggestions. D.S., E.K., and M.H. are grateful for support from the IEEE Program "Magnetism for Ukraine 2023" supported by the IEEE Magnetic Society and the Science and Technology Center in Ukraine (STCU) framework (Project No. 9918). A.S. acknowledges the financial support of the Internal Grant Agency of Brno University of Technology (Grant No. CEITEC VUT-J-19-6070), Czech Republic. O.L. and A.S. acknowledge the financial support of the Grant Agency of the Czech Republic (GAČR) (Project No. Standard 23-05578S). P.N. acknowledges the financial support of the Grant Agency of the Czech Republic (GAČR) (Project No. EXPRO 21-20716X).

[1] F. La Via, D. Alquier, F. Giannazzo, T. Kimoto, P. Neudeck, H. Ou, A. Roncaglia, S. E. Saddow, and S. Tudisco, Emerging SiC applications beyond power electronic devices, Micromachines **14**, 1200 (2023).

[2] Z. Chen and A. Q. Huang, Extreme high efficiency enabled by silicon carbide (SiC) power devices, Mater. Sci. Semicond. Process. **172**, 108052 (2024).

[3] X. Ding, J. Cheng, and F. Chen, Impact of silicon carbide devices on the powertrain systems in electric vehicles, Energies **10**, 533 (2017).

[4] D. G. Lamar, Latest developments in LED drivers, Electronics **9**, 619 (2020).

[5] Q. Zhou, X. Yin, H. Xu, M. Li, X. Fan, Z. Yu, F. Ye, L. Cheng, and L. Zhang, Design and fabrication of silicon carbides

reinforced composite with excellent radar absorption property in *X* and *Ku* band, J. Phys. D: Appl. Phys. **52**, 435102 (2019).

[6] L. Qian, Y. Baskaran, M. Krödel, C. M. España, L. Pambaguian, T. Skaik, and Y. Wang, Lightweight, high-Q and high temperature stability microwave cavity resonators using carbon-fiber reinforced silicon-carbide ceramic composite, IEEE J. Microwaves **3**, 1230 (2023).

[7] E. Hesselmeier, P. Kuna, I. Takács, V. Ivády, W. Knolle, N. T. Son, M. Ghezellou, J. Ul-Hassan, D. Dasari, F. Kaiser, V. Vorobyov, and J. Wrachtrup, Qudit-based spectroscopy for measurement and control of nuclear-spin qubits in silicon carbide, Phys. Rev. Lett. **132**, 090601 (2024).

[8] S. Majety, P. Saha, Z. Kekula, S. Dhuey, and M. Radulaski, Triangular cross-section beam splitters in silicon carbide for quantum information processing, MRS Commun. (2024), doi:10.1557/s43579-024-00557-0.

[9] S. Castelletto, C. Lew, W. X. Lin, and J. S. Xu, Quantum systems in silicon carbide for sensing applications, Rep. Prog. Phys. **87**, 014501 (2024).

[10] E. Hesselmeier, P. Kuna, W. Knolle, F. Kaiser, N. T. Son, M. Ghezellou, J. Ul-Hassan, V. Vorobyov, and J. Wrachtrup, High-fidelity optical readout of a nuclear-spin qubit in silicon carbide, Phys. Rev. Lett. **132**, 180804 (2024).

[11] R. Mickevičius and J. H. Zhao, Monte Carlo study of electron transport in SiC, J. Appl. Phys. **83**, 3161 (1998).

[12] V. V. Afanas'ev, A. Stesmans, M. Bassler, G. Pensl, and M. J. Schulz, Shallow electron traps at the 4H-SiC/SiO_2 interface, Appl. Phys. Lett. **76**, 336 (2000).

[13] Y. Shao, H. Hu, B. Zhang, X. Hao, and Y. Wu, Crystallographic orientation and strain in GaN crystals grown on 6H-SiC and sapphire substrates, Crystals **13**, 1694 (2023).

[14] A. Dobrowolski, J. Jagiełło, K. Piętak-Jurczak, M. Wzorek, D. Czołak, and T. Ciuk, Spectroscopic properties of close-to-perfect-monolayer quasi-free-standing epitaxial graphene on 6H-SiC(0001), Appl. Surf. Sci. **642**, 158617 (2024).

[15] M. Lesecq, Y. Fouzi, A. Abboud, N. Defrance, F. Vaurette, S. Ouendi, E. Okada, M. Portail, M. Bah, D. Alquier, J.-C. De Jaeger, E. Frayssinet, and Y. Cordier, Performance improvement with non-alloyed ohmic contacts technology on AlGaN/GaN high electron mobility transistors on 6H-SiC substrate, Microelectron. Eng. **276**, 111998 (2023).

[16] S. Kimura, H. Yoshida, S. Uchida, and A. Ogino, Thermionic emission and conversion properties of n-type AlGaN thin film cathodes grown on 6H–SiC substrates, Jpn. J. Appl. Phys. **59**, SGGF01 (2020).

[17] R. Lewandków, M. Grodzicki, P. Mazur, and A. Ciszewski, Properties of thin MgO films on 6H–SiC and GaN: Photoelectron studies, Acta Phys. Pol., A **141**, 116 (2022).

[18] X. M. Zhang, C. L. Yan, C. H. Zeng, Y. Q. Wang, B. S. Zhang, and C. Pang, Synthesis of diamond on SiC by microwave plasma chemical vapor deposition: Comparison of silicon-face and carbon-face, Mater. Sci. Forum **1014**, 8 (2020).

[19] S. Rashid, F. Bashir, F. A. Khanday, and M. R. Beigh, Double gate 6H-silicon carbide Schottky barrier FET as dielectrically modulated label free biosensor, Silicon **15**, 3387 (2022).

[20] A. Gottscholl, C. J. Cochrane, and H. Kraus, Operation modes of an optically pumped 6H SiC quantum/solid-state magnetometer, IEEE Sens. J. **24**, 17596 (2024).

[21] M. V. Muzafarova, I. V. Il'in, A. N. Anisimov, E. N. Mokhov, V. A. Soltamov, and P. G. Baranov, Electronic structure and spatial distribution of the spin density of shallow nitrogen donors in the SiC lattice, Semiconductors **58**, 2406 (2016).

[22] Y. Inoue, W. Tochizaki, T. Iwai, K. Tanabe, and N. Ohtani, Nitrogen doping concentration dependence of nitrogen incorporation kinetics during physical vapor transport growth of 4H–SiC crystals, Mater. Sci. Semicond. Process. **176**, 108266 (2024).

[23] C. J. Cochrane, P. M. Lenahan, and A. J. Lelis, Identification of a silicon vacancy as an important defect in 4H SiC metal oxide semiconducting field effect transistor using spin dependent recombination, Appl. Phys. Lett. **100**, 023509 (2012).

[24] Y. Abe, A. Chaen, M. Sometani, S. Harada, Y. Yamazaki, T. Ohshima, and T. Umeda, Electrical detection of T_{V2a}−type silicon vacancy spin defect in 4H-SiC MOSFETs, Appl. Phys. Lett. **120**, 064001 (2022).

[25] C. J. Cochrane, P. M. Lenahan, and A. J. Lelis, An electrically detected magnetic resonance study of performance limiting defects in SiC metal oxide semiconductor field effect transistors, J. Appl. Phys. **109**, 014506 (2011).

[26] J. P. Ashton and P. M. Lenahan, Multiple-photon transitions in electrically detected magnetic resonance measurements of 4H-SiC transistors, Phys. Rev. B **102**, 020101(R) (2020).

[27] R. J. Waskiewicz, B. R. Manning, D. J. McCrory, and P. M. Lenahan, Electrically detected electron nuclear double resonance in 4H-SiC bipolar junction transistors, J. Appl. Phys. **126**, 125709 (2019).

[28] P. M. Lenahan, N. T. Pfeiffenberger, T. G. Pribicko, and A. J. Lelis, Identification of deep level defects in SiC bipolar junction transistors, Mater. Sci. Forum **527–529**, 567 (2006).

[29] T. Umeda, Y. Nakano, E. Higa, T. Okuda, T. Kimoto, T. Hosoi, H. Watanabe, M. Sometani, and S. Harada, Electron-spin-resonance and electrically detected-magnetic-resonance characterization on P_{bC} center in various 4H−SiC(0001)/SiO_2 interfaces, J. Appl. Phys. **127**, 145301 (2020).

[30] E. Higa, M. Sometani, H. Hirai, H. Yano, S. Harada, and T. Umeda, Electrically detected magnetic resonance study on interface defects at nitrided Si-face, a-face, and m-face 4H-SiC/SiO_2 interfaces, Appl. Phys. Lett. **116**, 171602 (2020).

[31] G. Gruber, J. Cottom, R. Meszaros, M. Koch, G. Pobegen, T. Aichinger, D. Peters, and P. Hadley, Electrically detected magnetic resonance of carbon dangling bonds at the Si-face 4H-SiC/SiO_2 interface, J. Appl. Phys. **123**, 161514 (2018).

[32] T. Umeda, T. Kobayashi, M. Sometani, H. Yano, Y. Matsushita, and S. Harada, Carbon dangling-bond center (carbon Pb center) at 4H−SiC(0001)/SiO_2 interface, Appl. Phys. Lett. **116**, 071604 (2020).

[33] N. M. Reinacher, M. S. Brandt, and M. Stutzmann, Spin-dependent transport in SiC and III-V semiconductor devices, Mater. Sci. Forum **196–201**, 1915 (1995).

[34] N. T. Bagraev, D. S. Gets, E. N. Kalabukhova, L. E. Klyachkin, A. M. Malyarenko, V. A. Mashkov, D. V. Savchenko, and B. D. Shanina, Electrically-detected electron paramagnetic resonance of point centers in 6H-SiC nanostructures, Semiconductors **48**, 1467 (2014).

[35] A. Solodovnyk, O. Laguta, A. Prokhorov, M. Segantini, P. Neugebauer, S. Greulich-Weber, E. Kalabukhova, and D. Savchenko, Spin dynamics of exchange-coupled nitrogen donors in heavily doped n-type 15 SiC monocrystals:

Multifrequency EPR and EDMR study, Phys. Rev. B **107**, 155202 (2023).

[36] M. I. Grasa Molina, EPR-induced charge transport in highly doped crystalline n-type Silicon Carbide, Ph.D. Dissertation, Paderborn University, Paderborn, Germany, 2000.

[37] D. V. Savchenko, The electron spin resonance study of heavily nitrogen doped 6*H* SiC crystals, J. Appl. Phys. **117**, 045408 (2015).

[38] Yu. M. Tairov and V. F. Tsvetkov, Investigation of growth processes of ingots of silicon carbide single crystals, J. Cryst. Growth **43**, 209 (1978).

[39] W. Suttrop, G. Pensl, and W. J. Choyke, Hall effect and infrared absorption measurements on nitrogen donors in 6*H*-silicon carbide, J. Appl. Phys. **72**, 3708 (1992).

[40] G. C. Capitani, S. Di Pierro, and G. Tempesta, The 6*H*-SiC structure model: Further refinement from SCXRD data from a terrestrial moissanite, Am. Mineral. **92**, 403 (2007).

[41] K. Momma and F. Izumi, VESTA 3 for three-dimensional visualization of crystal, volumetric and morphology data, J. Appl. Crystallogr. **44**, 1272 (2011).

[42] A. Sojka, M. Sedivy, A. Lagin, A. Gabris, T. Laznicka, V. T. Santana, O. Laguta, and P. Neugebauer, Sample holders for sub-THz electron spin resonance spectroscopy, IEEE Trans. Instrum. Meas. **71**, 1 (2022).

[43] M. Šedivý, V. Santana, A. Sojka, O. Laguta, and P. Neugebauer, MEPROS–modular electron paramagnetic resonance operating software for multifunctional high-frequency EPR spectrometer, J. Magn. Reson. **355**, 107556 (2023).

[44] A. Solodovnyk, D. Savchenko, O. Laguta, and P. Neugebauer, Implementation of broadband electrically detected magnetic resonance in a sub-THz FraScan spectrometer, IEEE Trans. Instrum. Meas. **72**, 6006708 (2023).

[45] S. Stoll and A. Schweiger, EASYSPIN, a comprehensive software package for spectral simulation and analysis in EPR, J. Magn. Reson. **178**, 42 (2006).

[46] D. V. Savchenko, E. N. Kalabukhova, V. S. Kiselev, J. Hoentsch, and A. Pöppl, Spin-coupling and hyperfine interaction of the nitrogen donors in 6*H*-SiC, Phys. Status Solidi B **246**, 1908 (2009).

[47] A. Ferreira da Silva, J. Pernot, S. Contreras, B. E. Sernelius, C. Persson, and J. Camassel, Electrical resistivity and metal-nonmetal transition in $n-$type doped $4H-$SiC, Phys. Rev. B **74**, 245201 (2006).

[48] E. N. Kalabukhova, S. N. Lukin, and O. T. Sergeev, Electron spin resonance of technological coatings made of silicon carbide, Phys. Solid State **35**, 210 (1993).

[49] D. V. Savchenko, D. M. Yatsyk, O. M. Genkin, Y. F. Nosachov, O. V. Drozdenko, V. I. Moiseenko, and E. N. Kalabukhova, Electrical properties of highly nitrogen-doped 6*H*-SiC single crystals: Microwave cavity perturbation study, Semicond. Phys. Quantum Electron. Optoelectron. **26**, 030 (2023).

[50] See Supplemental Material at http://link.aps.org/supplemental/10.1103/PhysRevB.110.125205 for temperature dependence, power dependence, and current dependence of EDMR signal measured in 6*H*-SiC single crystals with N_D–$N_A \approx 8 \times 10^{18}\,\mathrm{cm}^{-3}$.

[51] R. Maxwell and A. Honig, Neutral-impurity scattering experiments in silicon with highly spin-polarized electrons, Phys. Rev. Lett. **17**, 188 (1966).